



Article

Mechanical High-Temperature Properties and Damage Behavior of Coarse-Grained Alumina Refractory Metal Composites

Anja Weidner ^{1,*}, Yvonne Ranglack-Klemm ¹, Tilo Zienert ² , Christos G. Aneziris ² and Horst Biermann ¹ 

¹ Institute of Materials Engineering, Technische Universität Bergakademie Freiberg, 09599 Freiberg, Germany; klemm_yvonne@web.de (Y.R.-K.); biermann@ww.tu-freiberg.de (H.B.)

² Institute of Ceramic, Glass and Construction Materials, Technische Universität Bergakademie Freiberg, 09599 Freiberg, Germany; tilo.zienert@ikgb.tu-freiberg.de (T.Z.); aneziris@ikgb.tu-freiberg.de (C.G.A.)

* Correspondence: weidner@ww.tu-freiberg.de; Tel.: +49-3731-39-2124

Received: 14 October 2019; Accepted: 24 November 2019; Published: 27 November 2019



Abstract: The present study provides the mechanical properties of a new generation of refractory composites based on coarse-grained Al₂O₃ ceramic and the refractory metals Nb and Ta. The materials were manufactured by refractory castable technology and subsequently sintered at 1600 °C for 4 h. The mechanical properties and the damage behavior of the coarse-grained refractory composites were investigated at high temperatures between 1300 and 1500 °C. The compressive strength is given as a function of temperature for materials with two different volume fractions of the refractory metals Ta and Nb. It is demonstrated that these refractory composites do not fail in a completely brittle manner in the studied temperature range. The compressive strength for all materials significantly decreases with increasing temperature. Failure occurred due to the formation of cracks along the ceramic/metal interfaces of the coarse-grained Al₂O₃ particles. In microstructural observations of sintered specimens, the formation of tantalates, as well as niobium oxides, were observed. The lower compressive strength of coarse-grained Nb-Al₂O₃ refractory composites compared to Ta-Al₂O₃ is probably attributed to the formation of niobium oxides. The formation of tantalates, however, seems to have no detrimental effect on compressive strength.

Keywords: refractory composites; high-temperature; mechanical properties; microstructure

1. Introduction

Ceramic–metal composites benefit from the combination of a high melting point, hardness and the chemical stability of ceramics, with the high toughness and ductility of metals. In general, the upper limit of the application temperature of such composites is restricted by the melting point of the metal, the reaction between the metal and ceramic particles, the chemical interaction with the environment, or the thermal mismatch between the ceramic and the metallic phases. Therefore, the use of refractory metals with a high melting point could make such composites applicable at even higher temperatures [1].

Typical refractory metals with a melting temperature above that of alumina ($T_m = 2054$ °C), are Mo, Nb, W, Ta, Hf, Tc, Re, Os, and Ir. Among them, Mo, Nb, W, and Ta are the most abundant [2,3]. Niobium and tantalum exhibit a similar coefficient of thermal expansion (CTE) as alumina in a wide temperature range [4]. For instance, Kirby et al. [4] showed that, between 1000 and 2000 °C, a linear increase of CTE occurred for all three materials, with $25\text{--}34 \times 10^{-6} \cdot \text{K}^{-1}$ for alumina, $24\text{--}30 \times 10^{-6} \cdot \text{K}^{-1}$ for niobium, and $20\text{--}25 \times 10^{-6} \cdot \text{K}^{-1}$ for tantalum. Accordingly, composites of alumina with tantalum

or niobium could be promising candidates for thermal shock resistant materials, as shown by some research groups [5–11]. Moreover, the interface between Nb and Al₂O₃ should be stable at high temperatures in an inert atmosphere [12–20]. Mechanical properties [6,7,10,11], wear behavior [21], chemical stability [19,22] and thermal conductivity [23] of the sintered mixtures of Nb and Al₂O₃ were reported only for components made of very fine powders. In particular, fine-grained tantalum-alumina composites were studied as a potential material for femoral head in total hip arthroplasty [24].

In the past, several investigations concerning high-temperature properties (creep, fracture toughness) were performed for Al₂O₃ ceramics [25,26], as well as refractory ceramics with up to 50% niobium [8,9,19,27–29]. In these papers, different damage mechanisms were discussed, e.g., ceramic-metal interface decohesion [8,29], fracture of ceramic particles [29], and retardation of crack propagation by a high-volume fraction of niobium [8,29], as well as the resulting high fracture toughness [9]. Furthermore, the formation of different intermetallic phases (AlNb₂, Al₃Nb) and niobium oxide (NbO) during (pressureless) sintering was reported [19,29]. However, the materials described in these papers are, without exception, fine-grained materials (particle size: Al₂O₃ < 100 μm, Nb < 50 μm) exhibiting high densities (>95%) [8] after the sintering or hot-pressing process.

In addition, there are studies on yttrium-stabilized, tetragonal zirconium dioxide, with 20 vol. % Nb [30,31], and zirconium dioxide/alumina, with 20 vol. % Ta [32], as well as zirconium dioxide, with 20 vol. % Nb and 20 vol. % Ta [33]. These materials were also very fine-grained composites with micro- to nano-sized particles. For this group of materials, improved fracture toughness was observed as reported for Ta- or Nb-added ceramics. The toughness results from two factors: (i) energy dissipation by the plastic deformation of the metallic components (Nb, Ta), and (ii) tetragonal to monoclinic phase transformation of the zirconium dioxide, which is accompanied by a volume expansion (approx. 4%) and generates compressive stresses.

Investigations on damage and crack growth at room temperature were carried out in several studies [8,28,32,33], on the basis of cracks generated by Vickers' indentation on the tensile-loaded surface of bending specimens. The crack-bridging effect, caused by plastic deformation of the metallic phases, was shown both for Ta and Nb.

Coarse-grained ceramic refractories are used in favor of fine-grained ceramic materials in high-temperature and metallurgical applications, due to their relatively high resistance to creep, thermal shock and corrosion resistance [34–38]. Furthermore, it was shown by Zienert et al. [39] that the shrinkage can be even further reduced by adding high melting refractory metals as fine matrix component. The sum of these promising results regarding the shrinkage behavior in combination with both good resistance to thermal shock, as well as the excellent electrical and thermal properties of these materials, offer the opportunity to selectively design individual parts of large-sized construction components. Thus, large components can be manufactured with negligible thermal stresses due to the negligible shrinkage behavior during sintering.

The aim of the present paper is to investigate a new generation of coarse-grained refractory composites [39] based on pre-synthesized coarse grains of a ceramic (Al₂O₃) and refractory metals (Nb, Ta). Considering their potential applications as, e.g., electrically controlled heat shields or non-wetting, electrically heatable crucible materials, experimental studies on their mechanical properties at high temperatures (in particular, compressive strength, creep, and stress-relaxation, as well as damage and fracture behavior) are necessary. Therefore, high-temperature mechanical properties under compressive loading of the coarse-grained refractory composites, based on coarse-grained alumina (up to 5 mm) and fine-grained niobium and tantalum, were investigated. The refractory composites were manufactured by powder metallurgical route with different volume fractions of tantalum or niobium. The mechanical properties were tested at 1300, 1400 and 1500 °C. In addition, compressive stress relaxation tests were performed. The microstructure of the tested materials was examined by scanning electron microscopy (SEM) and energy-dispersive spectroscopy (EDS).

2. Materials and Methods

2.1. Materials and Preparation

The materials under investigation were coarse-grained refractory composites based on coarse-grained alumina and fine-grained refractory metals niobium and tantalum. The following raw materials were used: tabular alumina T60/64 (Almatis GmbH, Frankfurt, Germany), reactive alumina CL370 (Almatis GmbH), alumina Martoxid MR-70 (Martinswerk GmbH, Bergheim, Germany), re-hydratable alumina binder Alphabond 300 (Almatis GmbH), dispersing aluminas ADS-1 and ADW-1 (Almatis GmbH), Nb powder (EWG E. Wagener GmbH, Heimsheim, Germany), Ta powder (haines & maassen Metallhandelsgesellschaft mbH, Bonn, Germany). The refractory metals were used as powders with a particle classification $d \leq 75 \mu\text{m}$, whereas the alumina used had different particle classifications (0–20 μm : 10 vol. %, 0–45 μm : 11 vol. %, 0–0.5 mm: 21 vol. %, 0.5–1 mm: 10 vol. %, 1–3 mm: 13 vol. %, and 2–5 mm: 24 vol. %). The two fractions with the smallest alumina particles (0–20 μm : 10 vol. %, 0–45 μm : 11 vol. %) were replaced by fine powder fractions (0–20 μm) of Ta and Nb, respectively, both with a purity of 99.95%. If both fractions of fine alumina particles were replaced by refractory metals composites with 21 vol. % of refractory metal resulted, whereas composites with 11 vol. % were obtained by replacing only one fraction of alumina (0–45 μm). Thus, Ta-Al₂O₃ composites and Nb-Al₂O₃ composites were manufactured with both 11 vol. % and 21 vol. % of refractory metals. The coarse-grained refractory composites were fabricated using a refractory castable technology consisting of a mixing procedure of powder mixtures with a volume of $\approx 350 \text{ cm}^3$ in a concrete mixer (ToniMAX, Toni Baustoffprüfsysteme GmbH, Berlin, Germany) using 5 mass% water and 1 mass% of dispersing alumina as additives. Produced castable blends were cast into prismatic (150 × 25 × 25 mm³) sample molds and remained there for 1 to 3 days. Hereafter, the samples were taken out and dried in air at 120 °C for 24 h, followed by a pressureless sintering regime under argon atmosphere at 1600 °C for 4 h. Heating rates of 3 K/min up to a temperature of 500 °C, and 10 K/min up to the sintering temperature of 1600 °C, were applied. Details of the chemical composition of the raw materials, the castable recipe and the castable technology were reported recently in [39]. Cylinders with a diameter of 15 mm and a height of 25 mm were prepared for the high-temperature mechanical tests from the sintered prism by hollow drilling. Since the mechanical tests (compression, stress–relaxation) require plane–parallel front faces, these faces were mechanically grinded using a special tool designed for this purpose (see Figure 1a). Therefore, the specimens were fixed by a semi-circular clamping part with well-defined geometry according to the diameter of the specimens. Subsequently, the upper and lower front faces (after turning the tool by 180° around the axis perpendicular to the cylinder axis) were ground. The porosity was determined before and after mechanical tests using both mercury porosimetry and the Archimedes' method.

2.2. Mechanical Testing

To investigate the mechanical behavior of the coarse-grained refractory composites, quasi-static compression and stress–relaxation tests were carried out on an electro-mechanical high-temperature 20 kN testing machine (Zwick/Roell, Neu-Ulm, Germany), as shown in Figure 1b. The compression tests were performed with a crosshead displacement rate of 15 $\mu\text{m/s}$ which results in an initial strain rate of about $7.5 \times 10^{-4} \text{ s}^{-1}$. The tests were carried out under argon atmosphere (gas-chamber: Maytec, Singen, Germany) after two evacuation cycles, in order to avoid oxidation of the metallic phases of the specimens. A detailed view of the specimen set-up and the heating system is shown in Figure 1c. The cylindrical specimen (1) is placed in a susceptor cage (6) between two Mo-based susceptors (5) (TZM alloy) to set a homogenous temperature distribution. The heating was performed by a water-cooled copper induction coil (2) controlled by a middle-frequency generator (Hüttinger HF 5010, Freiburg, Germany) with heating rates up to 20 K/s. Strain was measured with a high-temperature extensometer system with alumina rods (3). Si₃N₄-pistons (4) transfer the load from the pressure tubes to the shown setup. The specimens were tested at 1300, 1400, and 1500 °C. For the metallic components,

this corresponds to a homologous temperature of $0.43 \leq T_{\text{hom}} \leq 0.49$ for Ta, and $0.52 \leq T_{\text{hom}} \leq 0.60$ for Nb. The temperature was measured on the surface of the specimens using a pyrometer Metis MS09 (Sensortherm, Sulzbach, Germany). A dwell time of 5 min was allowed prior to the tests in order to guarantee a homogenous temperature distribution and to minimize the effects of thermal expansion of the susceptors on the strain measurement. One specimen was tested for each material composition (11 vol. % Ta or Nb and 21 vol. % Ta or Nb, respectively) and each temperature. It should be noted here that the authors are aware of scatter in mechanical data of ceramic materials. However, it is known from other ceramic materials, such as carbon-bonded magnesia (MgO-C), that the scatter of data decreases with an increase in the “pseudo ductility” of these materials at high temperatures, depending on the content of graphite. However, for these new coarse-grained Ta-Al₂O₃ and Nb-Al₂O₃, the Weibull distribution of the mechanical data cannot be provided due to limited material.

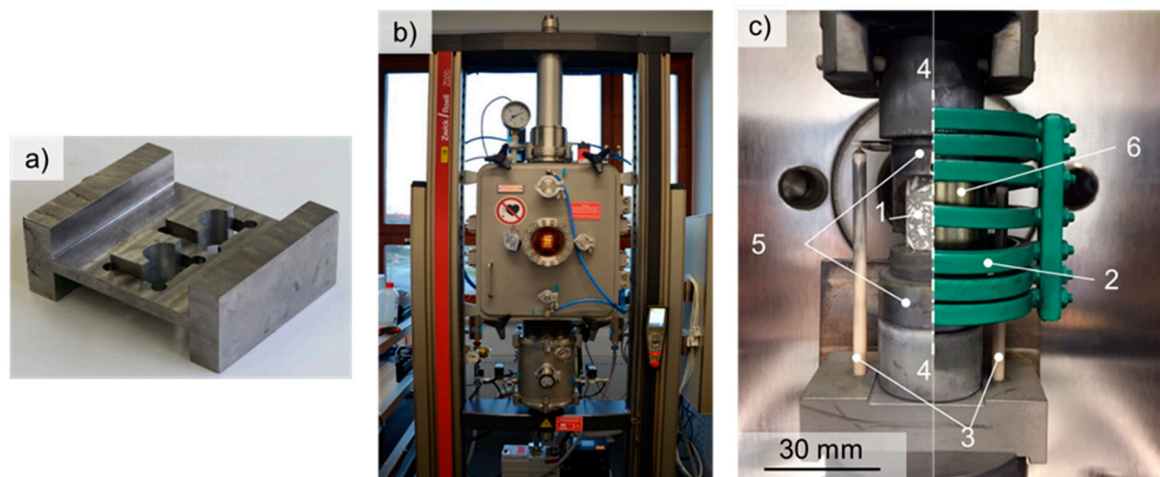


Figure 1. Setup for high-temperature testing of refractory metal-alumina composites. (a) Tool for manufacturing of plane-parallel front faces of cylindrical specimens for compression tests. (b) Testing machine with protective gas chamber. (c) Setup for compression tests. (1) Specimen. (2) Induction coil. (3) Alumina extensometer rods. (4) Si₃N₄ punches. (5) Susceptors. (6) Susceptor cage.

Stress relaxation tests were performed under compressive load at the same temperatures. The compressive load for the relaxation tests was chosen according to 80% of the maximum load achieved during the high-temperature compression tests.

2.3. Microstructural Investigations

The microstructure of the refractory composites was investigated before and after the compression tests, using a Scanning Electron Microscope (SEM), (Mira 3 XMU, Tescan, Brno, Czech Republic). SEM micrographs were taken in Secondary Electron (SE) or Back-Scattered Electron (BSE) contrast. In addition, Energy-Dispersive Spectroscopy (EDS) was performed in terms of point and line analysis, in order to study possible reactions of the refractory metals with alumina using EDS detector (Apollo 10 mm²) and acquisition software from EDAX.

3. Results and Discussion

3.1. Initial Microstructure of Refractory Metal-Alumina Composites

The microstructure of the specimens after the sinter process was investigated on cylindrical specimens cut parallel to the cylinder axis. Figure 2 shows exemplarily SEM micrographs of specimens, with 21 vol. % Ta and Nb, respectively. In Figure 2a, the coarse-grained fraction of alumina particles (>1 μm) is clearly visible, with pores remaining from the manufacturing process. Both the Ta and the Nb particles exhibit a good bonding with the alumina particles. However, in both materials, a reaction

between alumina and refractory metals seems to occur during the sintering process. Clear indicators for this assumption are the different grey levels found both beside Ta particles (Figure 2b), as well as Nb particles (Figure 2c).

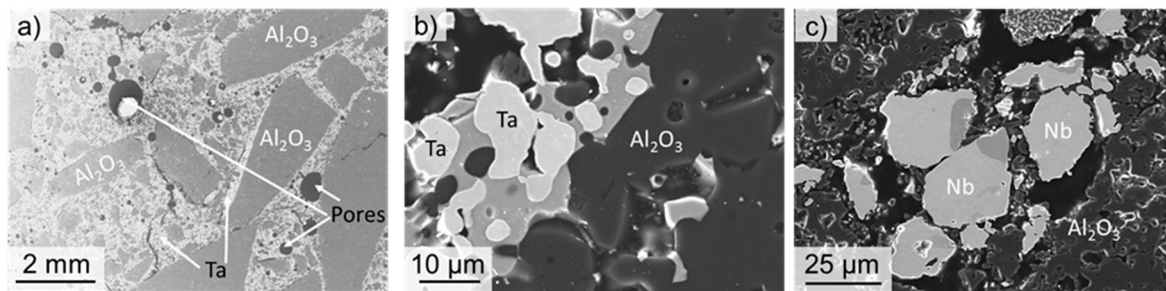


Figure 2. Microstructure of coarse-grained refractory metal-alumina composites after sintering at 1600 °C for 4 h. (a) Overview on microstructure of a specimen with 21 vol. % of Ta. (b,c) Details of microstructures of specimens with 21 vol. % Ta (b) and Nb (c), respectively, showing good bonding between alumina particles and refractory metal Ta (b) and Nb (c). In both cases, additional phases seem to develop during sintering. All micrographs in SE contrast.

To study the reaction of Ta and Nb with Al_2O_3 , EDS line measurements were performed on both microstructures. The results are summarized in Figures 3 and 4, for Nb and Ta refractory composites, respectively. It is clearly visible that, in the dark-grey area of Nb particles (cf. Figure 3a), an enrichment of oxygen was measured by EDS, whereas, in the brighter-grey area, nearly 100% of Nb was measured (cf. Figure 3b). This enrichment of oxygen in Nb was observed frequently in the microstructure and is most probably the result of the sintering process.

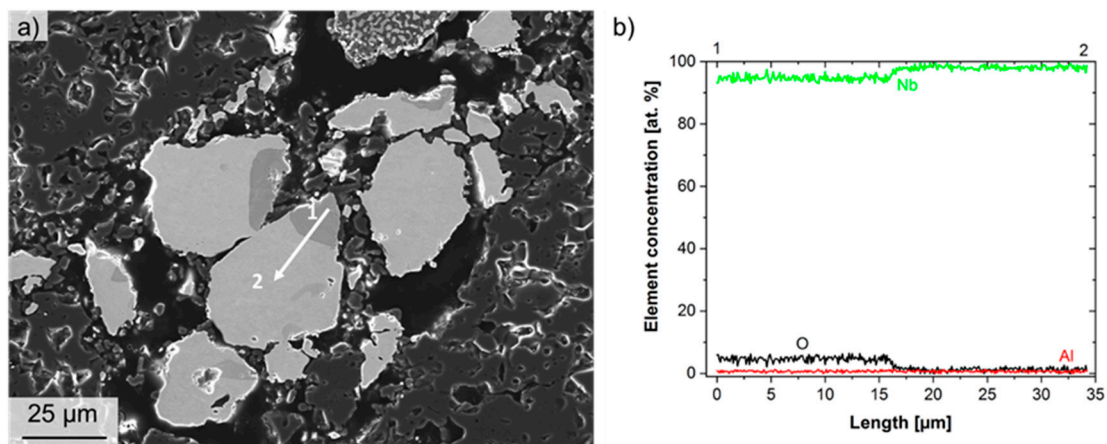


Figure 3. Results of energy-dispersive spectroscopy (EDS) analysis on a Nb particle. (a) Scanning electron microscopy (SEM) micrograph (SE contrast) with indicated position for EDS line analysis. (b) EDS line profile for the elements Nb, O and Al. Element concentrations are shown in at. %.

Similar behavior was found for Ta particles. Here, also different grey levels in the SEM micrograph (see Figure 4a) serve as an indicator for the formation of a new phase beside pure Ta and alumina. In contrast to Nb refractory composites, here, an enrichment not only of oxygen but also of aluminum was detected, as the EDS line profile shows in Figure 4b. Thus, a sequence from pure tantalum (bright-grey; 1) over pure alumina (dark-grey) to an area composed of O, Ta and Al (light-grey) to pure Ta again (bright-grey), ending in pure alumina (2), was detected. This frequently observed enrichment of oxygen and aluminum in Ta-particles is mostly attributed, as mentioned above, to the consequence of reactions during the sintering process.

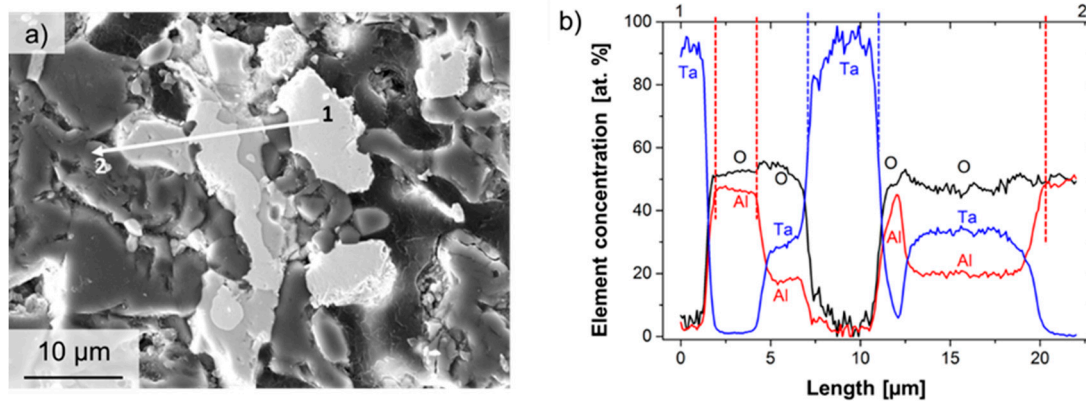


Figure 4. Results of EDS analysis on Ta particles. (a) SEM micrograph (SE contrast) with indicated position for EDS line analysis. (b) EDS line profile for the elements Ta, O and Al. Element concentrations are shown at. %.

It is assumed that this phase could be representative of the group of aluminum tantalates [40,41]. Tantalum has a high affinity for oxygen [42,43]. Tantalum powders, therefore, form a tantalum-(V)-oxide (Ta_2O_5) [42,43] at the surface. At higher temperatures (approx. 1300 °C), this oxide can react with Al_2O_3 to aluminum tantalate AlTaO_4 [40,41,44] (light-grey in Figure 4a). However, the ternary system Ta-Al-O is not yet well investigated regarding both the occurring phase equilibria as well as the thermodynamics. King et al. [45] and Roth and Waring [46] showed, for the subsystem Ta_2O_5 - Al_2O_3 , a solubility of about 10 mol. % Al_2O_3 in Ta_2O_5 , and the formation of an intermediate phase $-\text{TaAlO}_4-$ —with an extended range of solid solution, as reported by Yamaguchi et al. [47]. In addition, Huang et al. [24] showed for hot-pressed specimens (1450 °C, 1650 °C) that, for these temperatures, a diffusion of oxygen in Ta as well as, at 1650 °C, a diffusion of Al in tantalum, occurred, since the formation of an interphase layer was observed. However, a diffusion of Ta in Al_2O_3 was not observed [24]. In similar way, the formation of aluminum niobates of the form AlNbO_4 was expected [44] for the system Al_2O_3 -Nb. However, here the formation of niobium-oxide was observed, as reported earlier by other groups [19,29]. A maximum solubility of oxygen in niobium of 0.9 at. %, and the formation of different types of stable niobium oxides (NbO , NbO_2 , Nb_2O_5 and $\text{Nb}_{12}\text{O}_{29}$ [48]) were reported. The formation of different intermetallic phases like niobium-aluminides of types AlNb_2 and Al_3Nb , as mentioned in [19,29], was not observed in our SEM investigations.

3.2. High-Temperature Compression Behavior

Figure 5 shows the results of the high-temperature compression tests on the composites. Figure 5a,b show the stress vs. strain curves for 11 vol. % (a) and 21 vol. % (b) niobium, and Figure 5c,d for tantalum. It is noteworthy that the materials show at least some limited ductility and do not fail in a brittle manner after maximum strength, despite the high-volume fraction of coarse-grained alumina. In all cases, the stress–strain curves exhibit the highest strength and elongation for 1300 °C. The maximum strength decreases significantly with an increase in temperature. Furthermore, the increase in volume fraction of the refractory metals results in a significant decrease in strength. However, the ductility seems to be comparable. Figure 6 shows the dependence of maximum compression strength on temperature for all tested materials. In general, the compressive strength of the materials with 11 vol. % of Ta or Nb is higher compared to the materials with higher volume fraction of metals. Furthermore, the compressive strength decreases for all materials with an increase in temperature. For the lower volume fraction, the Ta-composite exhibits a higher strength than that with Nb. For the higher volume fraction, both composite materials show comparable strength values. However, the decrease in compressive strength with an increase in temperature is less pronounced for materials with a higher volume fraction of refractory metals. The elongation to failure decreases with an increase in temperature. Furthermore, it should be noted that the porosity of all materials is comparable before

and after mechanical testing, and lies in the order of about 17%, which means that no consolidation occurred during the high-temperature compression tests.

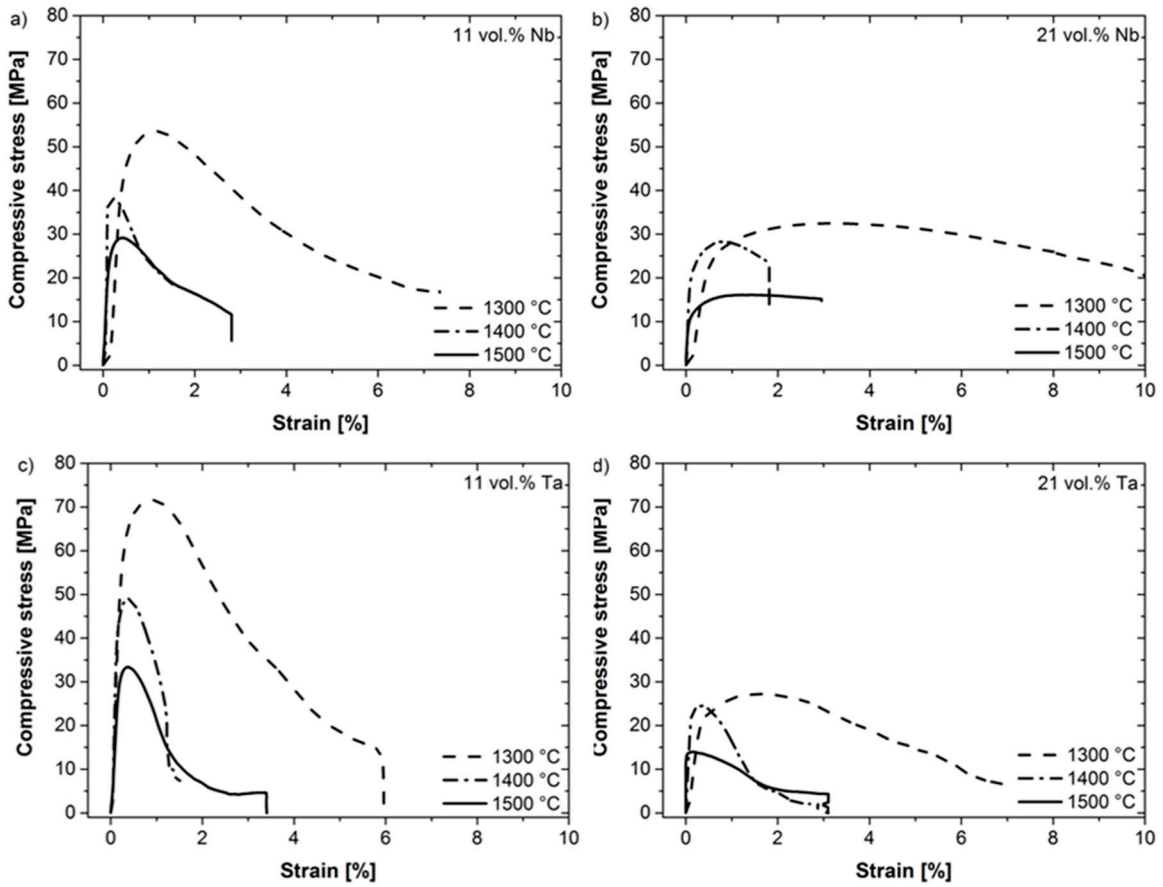


Figure 5. Results of the compression tests up to 1500 °C on coarse-grained Ta-Al₂O₃ and Nb-Al₂O₃ refractory composites with 11 vol. % (a,c) and 21 vol. % (b,d) Nb (a,b) and Ta (c,d), respectively.

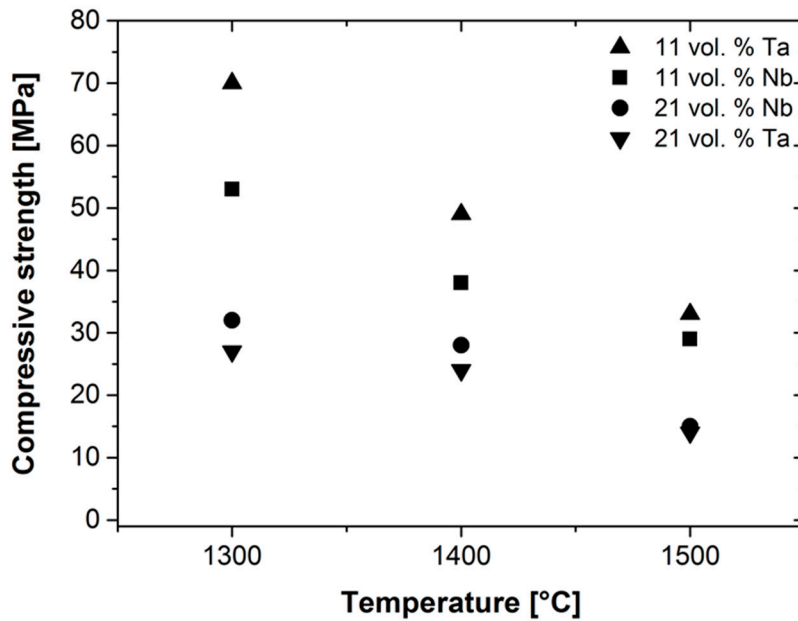


Figure 6. Compressive strengths of the coarse-grained Ta-Al₂O₃ and Nb-Al₂O₃ specimens at temperatures of 1300, 1400 and 1500 °C.

The macroscopic damage patterns of coarse-grained Ta-Al₂O₃ and Nb-Al₂O₃ specimens deformed at 1300 °C are summarized in Figure 7. The upper row of Figure 7 shows one of the two front faces, while the lower row shows side views of the cylindrical specimens. The coarse-grained Al₂O₃ with grain sizes up to 5 mm is clearly visible on the end faces. In addition, macro-porosity is visible. From the side views of the specimens it can be seen that the cracks run predominantly along the ceramic/metal interfaces. Furthermore, the specimens did not fail completely in a brittle manner; instead, some remaining ductility occurred. However, in all cases mechanical spallation of outer areas was observed.

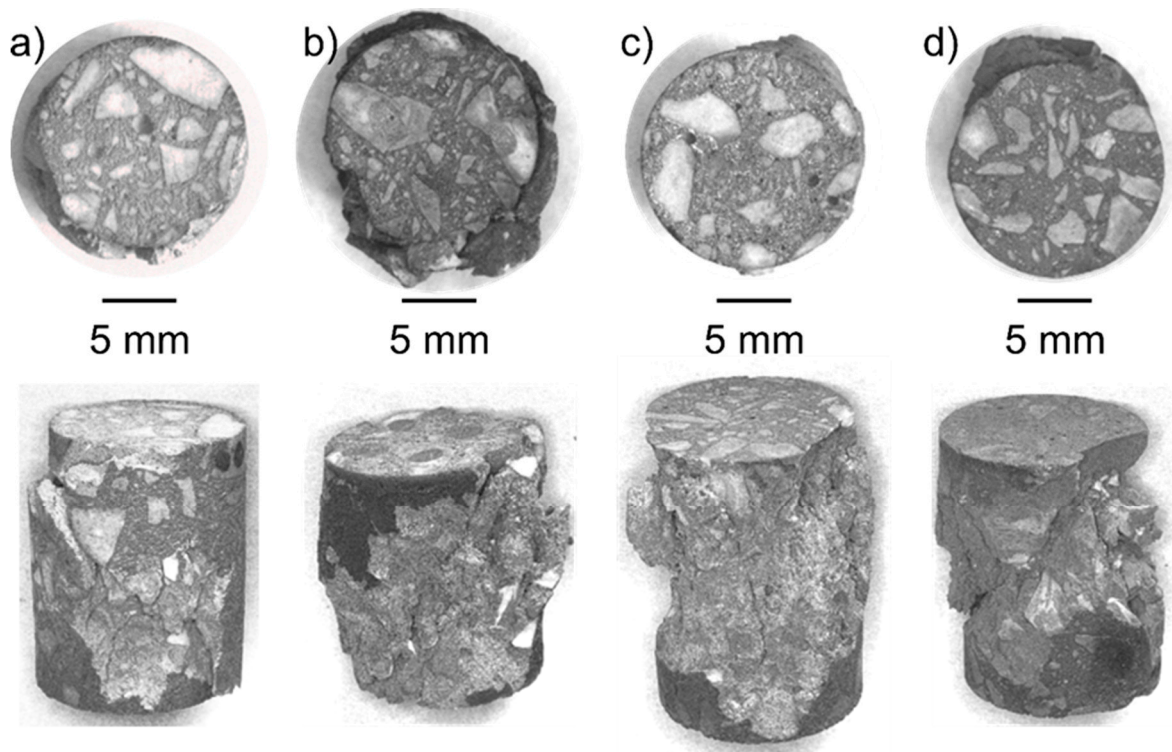


Figure 7. Specimens of coarse-grained Ta-Al₂O₃ and Nb-Al₂O₃ refractory composite materials with 11 vol. % and 21 vol. % Nb (a,b) and Ta (c,d), respectively, after compression tests at 1300 °C. Top: Front faces of cylindrical specimens (diameter: 15 mm, height: 22 mm). Bottom: Side views of the cylinders with macroscopic damage pattern.

The damage behavior was also investigated by SEM after the compression tests. Figure 8a,b show specimens with 11 vol. % Nb (a) and Ta (b), respectively, after compression tests at 1500 °C. The pronounced porosity and the severe damage of the microstructure with cracks running from pores along the interfaces between the large Al₂O₃ grains and the grains of the refractory metal can be clearly seen in both specimens. In addition, Figure 8d–f also reveal the damage behavior of the Nb particles. In particular, Nb particles with enrichment of oxygen seem to be favored for crack initiation. Thus, many tiny cracks (marked by black arrows) were observed in these areas indicating an embrittlement of the Nb particles by the formation of niobium oxides, which can be the reason for the lower strength of coarse-grained Nb-Al₂O₃ refractory composites compared to Ta-Al₂O₃ composites. The formation of fine Ta fringes along the grain boundaries of Al₂O₃ was observed (Figure 8c), indicating the diffusion of the refractory metals along the grain boundaries during the sintering process.

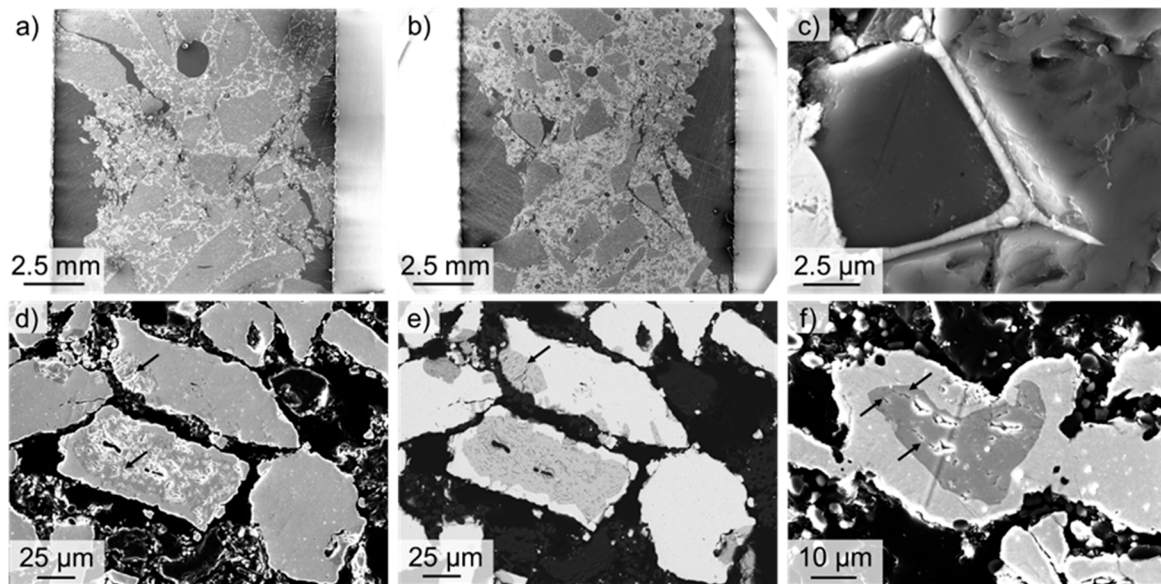


Figure 8. SEM micrographs of specimens after compression tests at 1500 °C. (a,b) Overview of the damaged microstructure of specimens with 11 vol. % Nb (a) and Ta (b). (c) Ta enrichment along the grain boundaries of Al₂O₃ (21 vol. % Ta). (d–f) Reaction of Al₂O₃ with Nb. (d,f) SE contrast. (e) BSE contrast.

Thus, the chemical bonding between alumina and refractory metals contributes to good mechanical properties in the Ta-Al₂O₃ and Nb-Al₂O₃ refractory composites compared to carbon-bonded oxides (MgO-C or Al₂O₃-C), where only a mechanical clamping between square-edged oxide particles contributes to the strength of these materials, since no chemical reaction between oxides and graphite occurs [49].

3.3. Stress-Relaxation Tests

In addition to the high-temperature compression tests, stress relaxation experiments were carried out at 1300 °C and 1500 °C. The initial compressive stresses were set to 80% of the maximum compressive stresses determined from the respective quasi-static compression tests (cf. Figure 5). The results of the relaxation tests are summarized in Figure 9. The samples with 11 vol. % Ta show the highest resistance to stress relaxation at 1300 °C, which corresponds to a homologous temperature of the metallic phase of $T_{\text{hom}} = 0.43$. Within the first 120 s, a stress drop of approx. 5–6 MPa occurs (approx. 10% of the stress). After that, only a small decrease in stress is observed, due to creep processes. For the higher testing temperature (i.e., $T_{\text{hom}} = 0.49$) a much stronger relaxation is observed (approx. 10 MPa stress drop, i.e., up to 30%). For the composite materials with 11 vol. % and 21 vol. % Nb, respectively, at 1300 °C and 1500 °C (equivalent to the homologous temperatures of Nb of $T_{\text{hom}} = 0.52$ and 0.6), a more pronounced relaxation behavior was observed within the first 3–4 min.

Specimens with 21 vol. % Nb show a stress relaxation only within the first few seconds, and a horizontal curve develops in the further course of the test, i.e., there are almost no further relaxation phenomena. The reason for the significant stress relaxation in all specimens within the first seconds or minutes is probably due to plastic deformation/dislocation rearrangement within the metallic components of the composite materials. It is highly probable that there are changes in the dislocation arrangement introduced by the initial compressive loading.

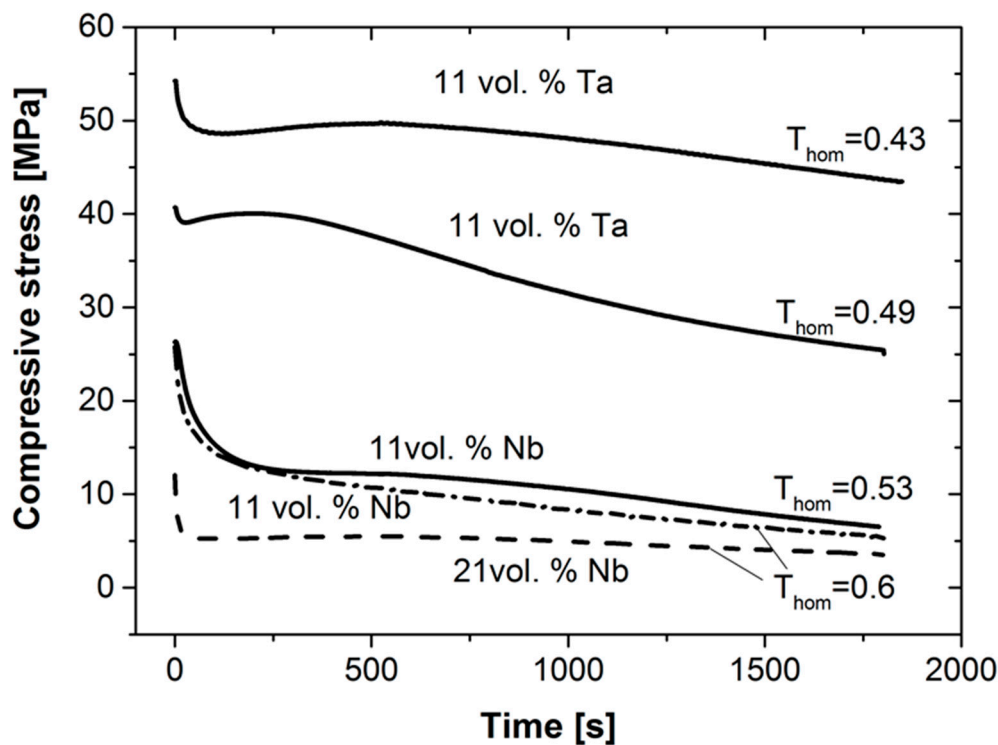


Figure 9. Results of compressive stress-relaxation tests performed on Ta-Al₂O₃ and Nb-Al₂O₃ specimens at 1300 °C and 1500 °C. The initial compressive loads were chosen with 0.8 of the experimentally determined maximum compressive strengths.

4. Summary

High-temperature mechanical properties were determined for the new class of coarse-grained refractory composites, based on Al₂O₃ and 11 or 21 vol. % of refractory metals Ta and Nb, respectively. It was demonstrated that these coarse-grained refractory composites do not fail in a completely brittle manner during compression tests between 1300 and 1500 °C. The compressive strength for all materials significantly decreases with an increase in temperature. Severe damage due to cracks running along the ceramic/metal interfaces of the coarse-grained Al₂O₃ particles was observed. The lower compressive strength of coarse-grained Nb-Al₂O₃ refractory composites compared to Ta-Al₂O₃ ones is probably attributed to the formation of niobium-oxides during the 4 h sinter process at 1600 °C. In contrast, the formation of tantalates seems not to have a detrimental effect on the compressive strength.

Author Contributions: Conceptualization, C.G.A. and H.B.; investigation, Y.R.-K., T.Z., A.W.; data analysis, Y.R.-K. and A.W.; writing—original draft preparation, A.W., T.Z., Y.R.-K.; writing—review and editing, A.W., H.B., C.G.A.; supervision, H.B., C.G.A.; project administration, C.G.A.

Funding: This research received no external funding.

Acknowledgments: The authors gratefully acknowledge the manufacturing of the coarse-grained refractory composites by Mahdi Farhani and Steffen Dudczig. Johannes Solarek is acknowledged for his support of performing high temperature compression tests.

Conflicts of Interest: The authors declare no conflict of interest.

References

1. Aneziris, C.G.; Homola, F.; Borzov, D. Material and Process development of Advanced Refractories for Innovative Metal Processing. *Adv. Eng. Mater.* **2004**, *6*, 562–568. [[CrossRef](#)]
2. Davis, J.R. *Heat-Resistant Materials*, 1st ed.; ASM International: Metals Park, OH, USA, 1997.
3. Schider, S. *Hochschmelzende Metalle: Pulvermetallurgische Werkstoffe für High-Tech-Anwendungen*; Verlag Moderne Industrie: Landsberg-Am Lech, Germany, 1990.

4. Kirby, R.K.; Hahn, T.A.; Rothrock, B.D. *American Institute of Physics Handbook-4f. Thermal Expansion*, 3rd ed.; McGraw-Hill Book Company: New York, NY, USA, 1972.
5. Kramer, C. *Thermal Shock Resistance of Al₂O₃ and Al₂O₃/Nb Cermets*; Sandia Labs.: Livermore, CA, USA, 1975; pp. 11–34.
6. Beals, J.; Nardone, V. Tensile behaviour of a niobium/alumina composite laminate. *J. Mater. Sci.* **1994**, *29*, 2526–2530. [[CrossRef](#)]
7. Shaw, L.; Miracle, D.; Abbaschian, R. Microstructure and mechanical properties of metal/oxide and metal/silicide interfaces. *Acta Metall. Mater.* **1995**, *43*, 4267–4279. [[CrossRef](#)]
8. García, D.; Schicker, S.; Janssen, R.; Claussen, N. Nb- and Cr-Al₂O₃ composites with interpenetrating networks. *J. Eur. Ceram. Soc.* **1998**, *18*, 601–605. [[CrossRef](#)]
9. García, D.; Schicker, S.; Bruhn, J.; Janssen, R.; Claussen, N. Processing and Mechanical Properties of Pressureless-Sintered Niobium-Alumina-Matrix Composites. *J. Am. Ceram. Soc.* **1998**, *81*, 429–432. [[CrossRef](#)]
10. Korn, D.; Ellsner, G.; Cannon, R.; Rühle, M. Fracture properties of interfacially doped Nb-Al₂O₃ bicrystals: I, fracture characteristics. *Acta Mater.* **2002**, *50*, 3881–3901. [[CrossRef](#)]
11. Thomson, K.; Jiang, D.; Yao, W.; Ritchie, R.; Mukherjee, A. Characterization and mechanical testing of alumina-based nanocomposites reinforced with niobium and/or carbon nanotubes fabricated by spark plasma sintering. *Acta Mater.* **2012**, *60*, 622–632. [[CrossRef](#)]
12. Morozumi, S.; Kikuchi, M.; Nishino, T. Bonding mechanism between alumina and niobium. *J. Mater. Sci.* **1981**, *16*, 2137–2144. [[CrossRef](#)]
13. Burger, K.; Mader, W.; Rühle, M. Structure, chemistry and diffusion bonding of metal/ceramic interfaces. *Ultramicroscopy* **1987**, *22*, 1–13. [[CrossRef](#)]
14. Mader, W.; Rühle, M. Electron microscopy studies of defects at diffusion-bonded Nb/Al₂O₃ interfaces. *Acta Metall.* **1989**, *37*, 853–866. [[CrossRef](#)]
15. Rühle, M.; Evans, A. Structure and chemistry of metal/ceramic interfaces. *Mater. Sci. Eng. A* **1989**, *107*, 187–197. [[CrossRef](#)]
16. Bruley, J.; Brydson, R.; Müllejans, H.; Mayer, J.; Gutekunst, G.; Mader, W.; Knauss, D.; Rühle, M. Investigations of the chemistry and bonding at niobium-sapphire interfaces. *J. Mater. Res.* **1994**, *9*, 2574–2583. [[CrossRef](#)]
17. Kapsa, R.; Matolín, M.; Gruzza, B. The AES and EELS study of thin alumina films deposited on niobium. *Vacuum* **1998**, *50*, 233–235. [[CrossRef](#)]
18. Sichinava, M.; Kobayakov, V. Interfacial reactions in layered composites of Nb-Al₂O₃ and Nb (1% Zr)-Al₂O₃ in high-temperature annealing. *Refract. Ind. Ceram.* **1999**, *40*, 203–207. [[CrossRef](#)]
19. Scheu, C.; Dehm, G.; Kaplan, W.D.; García, D.E.; Claussen, N. Microstructure of Alumina Composites Containing Niobium and Niobium Aluminides. *J. Am. Ceram. Soc.* **2000**, *83*, 397–402. [[CrossRef](#)]
20. McKeown, J.T.; Sugar, J.D.; Gronsky, R.; Glaeser, A.M. Effects of impurities on alumina-niobium interfacial microstructures. *Mater. Charac.* **2006**, *57*, 50–57. [[CrossRef](#)]
21. Portu, G.d.; Guicciardi, S.; Melandri, C.; Monteverde, F. Wear behaviour of Al₂O₃-Mo and Al₂O₃-Nb composites. *Wear* **2007**, *262*, 1346–1352. [[CrossRef](#)]
22. Grossman, L. Niobium-Al₂O₃ Reactions Yielding Condensed and Volatile Products. *J. Chem. Phys.* **1966**, *44*, 4127–4131. [[CrossRef](#)]
23. Santos, W.N.D.; Filho, P.I.P.; Taylor, R. Effect of addition of niobium oxide on the thermal conductivity of alumina. *J. Eur. Ceram. Soc.* **1998**, *18*, 807–811. [[CrossRef](#)]
24. Huang, T.; Rahaman, M.; Bal, B. Alumina–tantalum composite for femoral head applications in total hip arthroplasty. *Mater. Sci. Eng. C* **2009**, *29*, 1935–1941. [[CrossRef](#)]
25. Ferber, M.K.; Jenkins, M.G.; Tennery, V.J. Comparison of tension, compression, and flexure creep for alumina and silicon nitride ceramics. *Ceram. Eng. Sci. Proc.* **1990**, *11*, 1028–1045.
26. Robertson, A.G.; Wilkinson, D.S.; Cacerest, C.H. Creep and creep fracture in hot-pressed alumina. *J. Am. Ceram. Soc.* **1991**, *74*, 915–921. [[CrossRef](#)]
27. Scheu, C.; Dehm, G.; Kaplan, W.D.; Wagner, F.; Claussen, N. Microstructure and phase evolution of niobium-aluminide-alumina composites prepared by melt-infiltration. *Phys. Stat. Sol. A* **1998**, *166*, 241–255. [[CrossRef](#)]

28. Thomson, K.E.; Jiang, D.; Lemberg, J.A.; Koester, K.J.; Ritchie, R.O.; Mukherjee, A.K. In situ bend testing of niobium-reinforced alumina nanocomposites with and without single-walled carbon nanotubes. *Mater. Sci. Eng. A* **2008**, *493*, 256–260. [[CrossRef](#)]
29. Moya, J.S.; Diaz, M.; Gutiérrez-González, C.F.; Diaz, L.A.; Torrecillas, R.; Bartolomé, J.F. Mullite-refractory metal (Mo, Nb) composites. *J. Eur. Ceram. Soc.* **2008**, *28*, 479–491. [[CrossRef](#)]
30. Bartolomé, J.F.; Gutiérrez-González, C.F.; Pecharroman, C.; Moya, J.S. Synergistic toughening mechanism in 3Y-TZP/Nb composites. *Acta Mater.* **2007**, *55*, 5924–5933. [[CrossRef](#)]
31. Bartolomé, J.F.; Gutiérrez-González, C.F.; Torrecillas, R. Mechanical properties of alumina-zirconia-Nb micro-nano hybrid composites. *Compos. Sci. Technol.* **2008**, *68*, 1392–1398. [[CrossRef](#)]
32. Smirnov, A.; Bartolomé, J.F.; Kurland, H.D.; Grabow, J.; Müller, F.A. Design of a new zirconia–alumina–Ta micro-nanocomposite with unique mechanical properties. *J. Am. Ceram. Soc.* **2016**, *99*, 3205–3209. [[CrossRef](#)]
33. Smirnov, A.; Beltrán, J.I.; Rodríguez-Suarez, T.; Pecharromán, C.; Muñoz, M.C.; Moya, J.S.; Bartolomé, J.F. Unprecedented simultaneous enhancement in damage tolerance and fatigue resistance of zirconia/Ta composites. *Sci. Rep.* **2017**, *7*, 44922. [[CrossRef](#)]
34. Mocellin, A.; Kingery, W. Creep Deformation in MgO-Saturated Large-Grain-Size Al₂O₃. *J. Am. Ceram. Soc.* **1971**, *54*, 339–341. [[CrossRef](#)]
35. Cannon, W.R.; Sherby, O.D. Creep Behavior and Grain-Boundary Sliding in Polycrystalline Al₂O₃. *J. Am. Ceram. Soc.* **1977**, *60*, 44–47. [[CrossRef](#)]
36. Rice, R. Review—Ceramic tensile strength-grain size relations: Grain sizes, slopes, and branch intersections. *J. Mater. Sci.* **1997**, *32*, 1673–1692. [[CrossRef](#)]
37. Schafföner, S.; Aneziris, C.G. Pressure slip casting of coarse grain oxide ceramics. *Ceram. Int.* **2012**, *38*, 417–422. [[CrossRef](#)]
38. Fruhstorfer, J.; Demuth, C.; Goetze, P.; Aneziris, C.G.; Ray, S.; Gross, U.; Trimis, D. How the coarse fraction influences the microstructure and the effective thermal conductivity of alumina castables—An experimental and numerical study. *J. Eur. Ceram. Soc.* **2018**, *38*, 303–312. [[CrossRef](#)]
39. Zienert, T.; Farhani, M.; Dudczig, S.; Aneziris, C.G. Coarse-grained refractory composites based on Nb-Al₂O₃ and Ta-Al₂O₃ castables. *Ceram. Int.* **2018**, *44*, 16809–16818. [[CrossRef](#)]
40. Jasper-Tönnies, B.; Müller-Buschbaum, H.K. Synthese und Struktur von AlTaO₄. *Z. Anorg. Allg. Chem.* **1983**, *504*, 113–116. [[CrossRef](#)]
41. Harneit, O.; Müller-Buschbaum, H.K. AlTaO₄ mit AlNbO₄-Struktur. *Z. Anorg. Allg. Chem.* **1991**, *596*, 107–110. [[CrossRef](#)]
42. Vermilyea, D.A. The oxidation of tantalum at 50–300°C. *Acta Metall.* **1958**, *6*, 166–171. [[CrossRef](#)]
43. Voitovich, V.B.; Lavrenko, V.A.; Adejev, V.M.; Golovko, E.J. High-temperature oxidation of tantalum of different purity. *Oxid. Met.* **1995**, *43*, 509–526. [[CrossRef](#)]
44. Sych, A.M.; Golub, A.M. Niobates and Tantalates of trivalent elements. *Russ. Chem. Rev.* **1977**, *46*, 210–225. [[CrossRef](#)]
45. King, B.W.; Schultz, J.; Durbin, E.A.; Duckworth, W.H. *Some Properties of Tantalum Systems*; BMI-1106; United States Atomic Energy Commission: Germantown, MD, USA, 1956; Volume 13, pp. 1–39.
46. Roth, R.S.; Waring, J.L. Effect of oxide additions on the polymorphism of tantalum pentoxide III. Stabilization of the low temperature structure. *J. Res. Natl. Bur. Stand. A* **1970**, *74*, 485–493. [[CrossRef](#)]
47. Yamaguchi, O.; Tomihisa, D.; Uegaki, T.; Shimizu, K. Formation and transformation of δ-Ta₂O₅ solid solution in the system Ta₂O₅-Al₂O₃. *J. Am. Ceram. Soc.* **1987**, *70*, C335–C338. [[CrossRef](#)]
48. Massih, A.R.; Pérez, R.J. *Thermodynamic Evaluation of the Nb-O System*; Technical Report. PM 05-002 v2; Quantum Technologies AB: Uppsala, Sweden, 2006.
49. Solarek, J.; Himcinschi, C.; Klemm, Y.; Aneziris, C.G.; Biermann, H. Ductile behaviour of fine-grained, carbon-bonded materials at elevated temperature. *Carbon* **2017**, *122*, 141–149. [[CrossRef](#)]

